Condensation studies in membrane evaporation and sweeping gas membrane distillation

Shuaifei Zhao [a,*], Paul H.M. Feron [a], Zongli Xie [b], Jianhua Zhang [c], Manh Hoang [b]

[a] *CSIRO Energy Technology, P.O. Box 330, Newcastle, NSW 2300, Australia*

** Tel. +61-2-4960-6127; email: Shuaifei.Zhao@csiro.au*

[b] *CSIRO Materials Science & Engineering, Clayton, VIC 3168, Australia*

[c] *Institute of Sustainability and Innovation, Victoria University, Melbourne, Victoria 8001, Australia*

Abstract

Vapor transfer is an important phenomenon in various thermally driven membrane processes such as membrane distillation (MD), membrane evaporation and membrane condensation. In this study, we explore the mass transfer phenomena in sweeping gas membrane distillation (SGMD) by systematically investigating the effects of operational parameters on the process performance. It is found that mass transfer in SGMD is principally determined by both the evaporation temperature and the sweeping gas flow rate, and is significantly influenced by the operational parameters (i.e. fluid velocities) through multiple effects, including the boundary layer effect on both sides of the membrane, and the temperature polarization effect. We also prove that at low gas flow rates (i.e. insufficient gas vapor-holding capacity) the sweeping gas becomes saturated and water vapor forms droplets due to condensation on the gas side of the membrane. To the best of our knowledge, this is the first study reporting the interesting mass transfer phenomena in terms of vapor condensation and droplet re-evaporation in SGMD, which are of great significance for the heat and mass transfer in many thermally driven membrane processes using stripping gas.

Key words: Vapor transfer; membrane distillation; membrane evaporation; mass and heat transfer; sweeping gas membrane distillation; membrane contactor.

1. Introduction

Water vapor transfer is a crucial phenomenon in various thermally driven membrane processes such as membrane distillation (MD), membrane evaporation and membrane condensation. In these processes, the driving force comes from the water vapor partial pressure difference across the membrane. MD is often considered to be an efficient desalination alternative because of its high salt rejection and overwhelming ability to employ low-grade heat [1-4]. MD can be carried out with four different configurations: direct contact membrane distillation (DCMD), air gap membrane distillation (AGMD), vacuum membrane distillation (VMD) and sweeping gas membrane distillation (SGMD), depending on the method by which water vapor is recovered on the permeate side of the membrane. Among them, DCMD is the most studied configuration due to its simple operation. On the contrary, SGMD is the least used configuration probably because that an external condenser is required to collect the permeate which will incur extra costs by complicating the system [5].

Membrane evaporation has the same process principle as MD, i.e., mass and heat transfer in membrane evaporation and sweeping gas membrane distillation are essentially the same. The difference between membrane evaporation and MD is in that membrane evaporation is used for the concentration of thermo-sensitive solutions [6-8], while MD aims to obtain high quality water from the vapor [4, 5]. Therefore, there is no need to recover the water vapor on the permeate side in membrane evaporation. Compared with MD, membrane evaporation has received much less attention in the membrane research community.

Heat and mass transfer in MD, particularly in DCMD, have been intensively studied since the 1980s [1, 4, 5, 9-16]. However, less than 5% of MD publications deal with SGMD [5]. Work

on SGMD was first reported in 1987 and the effects of operational parameters on evaporation efficiency were studied [17]. After more than a decade, Khayet et al. conducted a series of experimental and modelling studies to further explore the influences of operational parameters on the process performance in SGMD [18-21]. In their work, the temperature profile along the membrane module and the temperature polarization in SGMD were explored by mathematical modelling [19, 20]. Recently, both response surface model and artificial neural network have been developed for the prediction and optimization of SGMD processes [22, 23].

Due to the limited amount of work on SGMD, there is a need to further explore the fundamental mass and heat transfer phenomena in this technology. This study aims to provide a new understanding on the fundamental mass transfer phenomena in SGMD. To clarify this understanding, here we focus on the mass transfer in SGMD, although the mass transfer and heat transfer are simultaneous in the process. Our new findings on the mass transfer phenomena will offer significant insights not only for SGMD but also for many other thermally driven membrane processes that use stripping gases.

2. Background

2.1. Relationships between vapor flux, vapor pressure and temperature

In thermally driven membrane processes such as membrane evaporation and SGMD, the driving force is the water vapor partial pressure difference across the membrane. As a result, the permeate flux (J_p) can be expressed as [9]

$$J_p = K_m\left(P_f - P_p\right) \quad (1)$$

where K_m is the mass transfer coefficient of a membrane, and P_f and P_p are the vapor partial pressures of the feed and permeate at the membrane surfaces, respectively. The vapor partial pressure of the feed solution (P_f) is a function of its temperature, and it can be estimated by the Antoine equation

$$P_f = exp\left(A - \frac{B}{C+t}\right) \quad (2)$$

where P_f is measured in mmHg and t in °C. For water (from 1 to 100 °C), A = 8.07131, B = 1730.63 and C = 233.42 [24, 25].

The vapor partial pressure of the sweeping gas is associated with the gas humidity ratio. Humidity ratio ω (i.e. mixing ratio or specific humidity) is defined as the ratio of the mass of water vapor (m_w) to the mass of dry gas (m_d)

$$\omega = \frac{m_w}{m_d} = \frac{M_w x_w}{M_d x_d} = \frac{M_w}{M_d}\frac{x_w}{1-x_w} \quad (3)$$

where M_w, M_d, x_w and x_d are the molar mass of water vapor, the molar mass of dry gas, the mole fraction of water vapor and mole fraction of dry gas, respectively.

Water partial vapor, dry gas and the mixture are assumed to obey the ideal gas law, i.e.:

$$P_w V = n_w RT \quad (4)$$

$$P_d V = n_d RT \quad (5)$$

$$(P_w + P_d)V = (n_w + n_d)RT \quad (6)$$

Therefore,

$$x_w = \frac{n_w}{(n_w+n_d)} = \frac{P_w}{P_w+P_d} = \frac{P_w}{P} \quad (7)$$

where P is the total pressure of the gas mixture, and n_w and n_d are the numbers of moles for the wet and dry gas, respectively.

Based on Eqs. (3) and (7), when using N_2 as the sweeping gas, the humidity ratio can be written as

$$\omega = \frac{0.643\ P_w}{P - P_w} \tag{8}$$

As a result, the vapor partial pressure on the gas side (i.e. permeate side) can be expressed as

$$P_p = P_w = \frac{\omega P}{\omega + 0.643} \tag{9}$$

Similarly, when using air as the sweeping gas,

$$P_p = P_w = \frac{\omega P}{\omega + 0.622} \tag{10}$$

In reality, the vapor partial pressure, humidity ratio and permeate flux associated with the temperature along the membrane surface are not homogenous. In modelling, however, these parameters are often supposed to change homogenously along the membrane based on a series of assumptions [18, 19].

2.2. Mass transfer mechanisms through a porous membrane

Mass transfer through a hydrophobic porous membrane has been interpreted by various mechanisms: the Knudsen diffusion model, viscous (Poiseuille) flow model, ordinary molecular (Fickian) diffusion model, and/or the combination thereof. The dominating mechanism is generally determined by the Knudsen number (K_n), which is defined by

$$K_n = \frac{\lambda}{d_{pore}} \tag{11}$$

where λ is the mean free path of the transferred gas molecule and d_{pore} is the mean pore diameter of the membrane (often in the range of 0.1~1.0 μm). The mean free path of a gas can be expressed by

$$\lambda = \frac{k_B \mathrm{T}}{\sqrt{2}\pi\sigma^2 P} \tag{12}$$

where k_B is the Boltzmann constant - 1.38×10^{-23} J/K; σ is the collision diameter of the molecule (2.641Å for water vapor); P is the pressure in Pa [12].

For the binary mixture of water vapor and air, the mean free path of water vapor in air ($\lambda_{w\text{-}a}$) at the average membrane temperature (T_m) can be estimated by [26]

$$\lambda_{w-a} = \frac{k_B \mathrm{T_m}}{P\pi\left(\frac{\sigma_w+\sigma_a}{2}\right)^2}\frac{1}{\sqrt{1+(M_w/M_a)}} \tag{13}$$

where σ_w=2.641 Å, σ_a=3.711 Å [27], and m_w and m_a are the molecular mass of water and air, respectively.

When the mean free path of the gas becomes larger than the pore size (i.e. K_n>1), molecule-wall collisions dominate the mass transfer which can be interpreted by the Knudsen diffusion using the following equation [1, 28, 29]

$$J_p = \frac{D_{Kn}}{RT\delta}\Delta P \tag{14}$$

with

$$D_{Kn} = \frac{4}{3} d_{pore}\frac{\varepsilon}{\tau}\sqrt{\frac{RT}{2\pi M_w}} \tag{15}$$

where D_{Kn} is the Knudsen diffusion coefficient, ε, τ and δ are the membrane porosity, tortuosity and thickness, respectively, R is the universal gas constant, T is the absolute temperature, m_w is the molecular weight of water, and $\Delta P = P_f - P_p$.

The viscous (Poiseuille) flow model is based on laminar flow which is determined by the gradient of the total pressure (i.e. pressure drop) across the membrane pore that is assumed to be cylindrical. Mass transfer can be described by

$$J_p = D_V \Delta P \tag{16}$$

with

$$D_V = \frac{1}{8}\frac{r^2 \varepsilon}{\delta \tau}\frac{M_w P_m}{\eta RT} \tag{17}$$

where D_V is the viscous flow coefficient, P_m is the average hydraulic pressure in the membrane pore, and η is the vapor viscosity. As the hydraulic pressure drop across the membrane pore in MD is very small, viscous flow is often negligible (i.e. not considered).

If the mean free path is much smaller than the pore size (i.e. $K_n<0.01$), molecule-molecule collisions become more significant and the mass transfer resistance is caused by the stagnant air trapped within the membrane pore. In this case, water vapor flux can be described by molecule diffusion [4, 10, 18]:

$$J_p = D_M \Delta P \tag{18}$$

with

$$D_M = \frac{1}{P_{air-lm}}\frac{\varepsilon}{\delta \tau}\frac{M_w DP}{RT} \tag{19}$$

where D_M is the molecular diffusion coefficient, $P_{air\text{-}lm}$ is the logarithmic mean pressure of air, D is the water vapor diffusion coefficient and P is the total pressure inside the membrane pore.

When $0.01<K_n<1$, mass transfer through a porous membrane can be explained by a combined Knudsen-molecular diffusion mechanism.

$$J_p = D_C \Delta P \tag{20}$$

with

$$D_C = \frac{M_w}{RT}\frac{1}{\delta}\left(\frac{1}{D_K}+\frac{P_a}{D_0}\right)^{-1} \tag{21}$$

where D_C is the combined Knudsen-molecular diffusion coefficient, P_a is the air pressure and $D_0=DP\varepsilon/\tau$.

According to Eqs. (11) and (13), Knudsen numbers of some typical porous membranes for MD at different temperatures are summarized in Table 1. It can be seen that Knudsen number increases gradually as evaporation temperature rises, but drops significantly as the membrane pore size increases. In most MD operations, the combined Knudsen-molecular diffusion mechanism dominates the mass transfer [18, 28]. However, when membrane pore size $d_{pore} \leq$ 0.1 μm, Knudsen diffusion becomes dominant in the mass transfer of the process.

3. Materials and methods

3.1. Membranes and characterization

Two types of flat sheet hydrophobic membranes (Dagong Co. Ltd., China) were used in our SGMD experiments. Each membrane consists of a polytetrafluoroethylene (PTFE) active layer and a polypropylene (PP) support layer with a grid-like structure. Data on membrane

pore sizes, liquid entry pressures and porosities were provided by the manufacture. The thicknesses of the active layer and support of the membrane were measured by a digital micrometer (Mitutoyo, Japan). The water contact angles of the membrane (active layers) were measured using a contact angle analyzer (DataPhysics Instruments GmbH, Filderstadt, Germany). The properties of the two types of PTFE membranes are summarized in Table 2, to give readers an overview of the membranes.

3.2. Experimental setup for membrane evaporation

Membrane evaporation experiments were conducted with a bench-scale membrane system as depicted in Fig. 1. The PTFE membrane cell has symmetric channels on both sides of the membrane, each channel with dimensions of 92.1, 45.7 and 2.3 mm for length, width and height, respectively. The membrane placed in the cell has an effective area of 42 cm^2. Dry or wet nitrogen was used as the sweeping gas, and its flow rate was measured with a flowmeter (Swagelok, Australia). Inlet/outlet gas humidities were measured by a humidity transmitter (Vaisala, Finland). Inlet/outlet temperatures of gas and liquid streams were monitored by K-type thermal couples (RS, Australia), and the gas inlet temperature was kept at room temperature (~ 21 °C). The thermal data was recorded with a data logger (Pico Technology, UK), and was controlled to within ± 0.2 °C. On the hot liquid side, pure water was heated in a thermoregulated bath and circulated with a gear pump (Process Pump, Australia). Another flow meter (Swagelok, Australia) was used to monitor the liquid flow rate. The liquid and the gas flowed counter-currently in each channel on both sides of the membrane. The weight loss of the liquid was measured by a balance (John Morris Scientific, Australia). The system (gauge) pressure on the gas side was zero (i.e. open system) and the system (gauge) pressure on the liquid side was ~13.8 kPa (2 psi), controlled by a pressure valve (Swagelok, Australia).

In the current study, it should be noted that the temperature change for the liquid water along the membrane is relatively small (maximum value ~ 0.5 °C) and that we selected the average temperature of the liquid inlet and outlet temperatures as the evaporation temperature.

3.3. Vapor pressure, humidity and flux determination

Gas vapor partial pressure is closely related to the gas temperature, pressure and humidity. In our study, the (saturated) vapor pressure and humidity of nitrogen were simulated by humidity calculation software (version 2.2, Vaisala, Finland).

In membrane evaporation and SGMD, water vapor and its associated heat permeate from the hot liquid to the cold sweeping gas as a result of the vapor partial pressure difference. The vapor flux can be obtained by the following equation:

$$J_p = \frac{\Delta W}{\Delta t\, A} \qquad (22)$$

where ΔW is the weight change (kg) during a time period Δt (h), and A is the effective membrane area (m^2). The unit of vapor flux is kg/m^2h.

Weight data were recorded at a time interval of 5 min for at least 50 min. The average value was used for the flux plotting and the calculated deviation was used as the error bar. It was found that the error bars were overlapped under some conditions due to the slight fluctuations in the experimental parameters. However, the overall trends of the mean values still revealed the influence of the operation conditions on mass transfer.

Additionally, vapor flux in SGMD could be related to the humidity change, and the following equation has been used for flux determination [18, 20]:

$$J_p = \frac{(\omega_{g,\ out} - \omega_{g,\ in})\dot{m}_g}{A} \qquad (23)$$

where $\omega_{g,\,out}$ and $\omega_{g,\,in}$ are the outlet and inlet gas humidity ratios (g/kg), respectively, and $\dot{m}_g$ is the mass flow rate of the sweeping gas (kg/h). It must be noted that Eq. (23) is only valid for unsaturated gas streams.

4. Results and discussion

Firstly, it is necessary to mention that all the following results are based on the observed experimental conditions, under which there was neither liquid leaking into the gas side nor sweeping gas penetrating into the liquid side, namely, no membrane wetting occurs due to the very low liquid side pressure (13.8 kPa, one order of magnitude lower than the liquid entry pressure of a typical MD membrane).

4.1. Effect of evaporation temperature on mass transfer in SGMD

In SGMD, evaporation temperature determines the vapor partial pressure difference across the membrane; hence it plays an important role in mass transfer. Fig. 2 shows the effect of evaporation temperature on the vapor flux in SGMD. The blue line represents the theoretical vapor pressure change with the evaporation temperature based on Eq. (3). Obviously, the membrane with larger pore size (0.45 μm) provided higher vapor flux than that with smaller pore size (0.1 μm), indicating the membrane with larger pore size has lower mass transfer resistance. This observation agrees well with the following fluid velocity investigation. It can also be seen that changes in vapor flux follow a similar trend with vapor partial pressure at a given evaporation temperature, as expected. However, the temperature at the membrane surface on the gas side also increases with the increase of the evaporation temperature due to simultaneous heat and mass transfer (as shown in Table 3), leading to an increase in the vapor partial pressure on the gas side. As a result, the vapor flux change trend as a function of the temperature is not exactly the same with the vapor partial pressure change. This difference is

more obvious at higher evaporation temperatures (Fig. 2) because the temperature of the gas becomes much higher at higher evaporation temperatures (Table 3).

Based on the experimental vapor flux, the outlet gas humidity ratio was determined using Eq. (23). The experimentally determined humidity ratio and simulated saturation humidity ratio (using the humidity calculation software from Vaisala) at the outlet of the sweeping gas were compared in Table 3. The experimentally determined humidity ratio at the outlet of the sweeping gas increases as a result of the increase in vapor flux with the evaporation temperature. The saturated humidity ratio also increases as a result of the increase in gas temperature associated with the heat transfer in membrane evaporation. However, it is interesting to note that the experimentally determined humidity is much higher than the saturated humidity at all temperatures. This means that we cannot use Eq. (23) for the calculation of the outlet gas humidity because the vapor in the membrane cell might be saturated. This is further illustrated by the results in the following sections.

4.2. Effect of gas flow rate on mass transfer in SGMD

Fig. 3 shows the effect of gas flow rate on the vapor flux in SGMD. As we can see, the sweeping gas flow velocity has a favourable effect on the vapor flux. This is principally determined by the fact that increasing the sweeping gas flow rate means enhancing the vapor-holding capacity of the gas but reducing the vapor partial pressure of the gas within the module. As the gas flow rate increases from 10 to 60 L/h, the vapor flux increases almost linearly for the two types of PTFE membranes. At higher gas flow rates, it seems that the vapor flux increase trends become not as sharp as that at lower gas flow rates, particularly for the membrane with smaller pore size. A further increase in gas flow rate does not have an effect as large since the partial pressure of water vapor has been reduced quite a bit already. It is also expected as a result of the boundary layer effect. At lower gas flow rates, the boundary

layer is supposed to be much thicker and more severe. And it is easier to be influenced by the change of the gas flow rate. At higher gas flow rates, the boundary layer effect has been minimised. Therefore, further increase in the gas flow rate does not have an effect as large as that at lower gas flow rates.

In Fig. 4, the relationship between the gas flow rate and the overall mass transfer coefficient also confirms the boundary layer effect. At lower gas flow rates, the overall mass transfer coefficient is more sensitive to the gas flow rate (larger slope reflected in Fig. 4) due to the more severe boundary layer effect.

The gas flow rate influences vapor flux likely by influencing the boundary layer at the active layer on the gas side (illustrated in Fig. 8). A higher gas flow rate could cause a thinner boundary layer and thus reduces the overall mass transfer resistance. The gas flow rate affects vapor flux also likely by influencing the temperature polarization effect [20], which still occurs at the active layer. Additionally, at higher gas flow rates, the transferred water vapor could be removed out of the module more effectively by lowering the pressure on the gas side via the Bernoulli effect, which will further facilitate the mass transfer across the membrane.

In addition, we also calculated the outlet gas humidity ratio using Eq. (23) based on the experimental vapor flux. The experimentally determined humidity ratio and simulated saturation humidity ratio at the outlet of the sweeping gas were summarized in Table 4. It can be seen that as the gas flow rate increases from 10 to 250 L/h, the temperature at the outlet of the gas increases slightly and then declines a little. The outlet temperature of the sweeping gas should decrease with the increase of the gas flow rate, namely more heat is swept away. However, there is more heat transferred to the gas side associated with the higher vapor flux at higher gas flow rate. This explains why the outlet temperature of the gas could increase or decrease with the increase of the gas flow rate. The corresponding saturated vapor and

saturated humidity have the same trend with the gas temperature as shown in Table 4. However, the experimentally determined humidity ratio decreases dramatically with the increase of the gas flow rate. More interestingly, all the experimentally determined humidity ratios are higher than the corresponding saturated humidity ratios. This suggests that Eq. (23) cannot be used for the humidity calculation because the sweeping gas has been super-saturated and that part of the vapor was condensed in the module, which was experimentally observed (Fig. 6). In particular, at lower gas flow rates the experimentally determined humidity ratios are much higher than the saturated humidity ratios, indicating the sweeping gas could become saturated once it contacts the permeated water vapor at lower gas flow velocities.

The occurrence of water vapor condensation on the gas side can be explained by the relatively low gas flow rates. At low gas flow rates, the vapor-holding capacity of the sweeping gas is relatively low and thus the sweeping gas cannot hold all the water vapor coming from the hot liquid, leading to vapor condensation. With the increase of the gas flow rate, the vapor-holding capacity of the sweeping gas increases and results in smaller difference between the experimentally determined humidity ratio and the saturated humidity ratio (Table 4). Additionally, the temperature drop between the transferred water vapor and the sweeping gas also contributes to the vapor condensation.

4.3. Effect of liquid flow rate on mass transfer in SGMD

Since boundary layers could occur on both sides of a membrane, the fluid hydrodynamic conditions on both sides will affect mass transfer in SGMD. The effect of liquid flow rate on the mass transfer in SGMD is shown in Fig. 5. It can be seen that the vapor flux increases as the liquid flow rate increases from 10 to 60 L/h. This is also regarded as a result of the boundary effect. However, the favorable effect of the liquid flow rate on the mass transfer is

not as significant as that of the gas flow rate on the mass transfer seen in Fig. 3. This suggests the boundary layer on the liquid side could be less significant but more intractable compared with the boundary layer on the gas side. This is caused by the diffusion coefficient differences between gases and liquids. Generally liquid diffusion coeffecients are 3 ~ 4 orders of magnitude lower than gas diffusion coeffients [27]. This can also lead to a much thinner boundary layer on the liquid side than that on the gas side as illustrated in Fig. 8. Khayet et al. ignored the effect of liquid flow rate on mass transfer in SGMD possibly because of the much thinner boundary layer on the liquid side at higher liquid rates [18, 19].

Similarly, we also compared the experimentally determined humidity ratio and the saturated humidity ratio at the outlet of the sweeping gas (Table 5). Both the temperature and saturated humidity at the outlet of the gas rise slightly as the liquid flow rate increases due to the increase in heat associated with the slightly higher vapor flux at greater liquid flow rates. The humidity determined from the experimental vapour flux has a similar trend. However, the experimentally determined humidity ratios are higher than the corresponding saturated humidity ratios. This further confirms that the gas in the membrane cell is saturated and droplets can form on the gas side of the membrane, as proven visually in Fig. 7 and explained conceptually in Fig. 8.

4.4. Comparison of the mass transfer using dry and humidified sweeping gases

To provide further support for the conclusion reached in the previous section, we also used humidified nitrogen as the sweeping gas. Fig. 6 shows the vapor flux using both dry and humidified nitrogen as the sweeping gas. It is surprising to find that dry and humidified gases have different influences at different gas flow rates. At lower gas flow rates humidified nitrogen provides higher vapor fluxes, more obvious for the membrane with larger pore size (0.45 μm). However, as the gas flow rate rises, dry nitrogen provides higher vapor fluxes.

Theoretically, the gas with lower humidity (e.g. dry gas) should provide a higher flux because of larger vapor pressure difference across the membrane. However, Khayet et al. reported that dry gas provided a lower flux than water saturated gas [19]. This variation in results is likely caused by the difference in the methods that were used for the flux calculation. We determined the vapor flux based on the weight loss on the liquid side, while Khayet calculated the flux according to the condensed water collected from the gas side, which could underestimate the vapor flux.

There could be an affinity between the vapor (within or close to the boundary layer) and the water molecule within the sweeping gas. At low gas flow rates, this affinity becomes obvious because of the weak hydrodynamic conditions. This may facilitate the water molecule diffusion between the membrane interface and the wet gas, as well as influence the boundary layer on the gas side. Such an affinity does not exist for dry gas. As a result, humidified gas provides higher vapor fluxes at lower gas flow rates.

Another explanation is related to the difference in the thermo-physical properties of nitrogen and water vapor. Water vapor has higher heat capacity and higher thermal conductivity than dry nitrogen (~ 1.9 vs. 1.0 $kJ \cdot kg^{-1} \cdot K^{-1}$ for heat capacity, and ~ 0.047 vs. 0.026 $W \cdot m^{-1} \cdot K^{-1}$ for thermal conductivity) [30]. Compared with dry nitrogen humidified nitrogen is therefore more prone to uptake heat from the boundary layer at the membrane interface. After heat coming out of the boundary layer, the temperature and vapor pressure at the membrane interface on the gas side will decrease, resulting in higher effective driving force and flux. However, as the gas flow rate increases, more and more gas goes along the membrane and vapor pressure difference becomes dominant in the mass transfer. Therefore, dry gas provides higher vapor fluxes at higher gas flow rates.

4.5. Mechanisms of the mass transfer in SGMD

After the experimental run using dry nitrogen as the sweeping gas, first we replaced the hot liquid with room-temperature water to retard water evaporation and vapor transfer, and then simultaneously turned off the sweeping gas and the circulation pump. Next, we opened the membrane cell and observed that droplets formed on the membrane support layer and in the membrane cell on the gas side (see Fig. 7). This important phenomenon directly proves that the gas stream in the module is saturated and that the transferred vapor forms droplets on the gas side due to condensation in SGMD processes [31]. Under gas stripping, the condensed droplets will re-evaporate and be swept out of the membrane module.

According to the above results and discussion, the mass transfer in SGMD was schematically illustrated in Fig. 8. Under the driving force of vapor partial pressure difference across the membrane, water vapor transports from the hot liquid side into the cold sweeping gas side. The mass transfer in this process is influenced by the hydrodynamic conditions on both sides of the membrane. The mass transfer resistance is principally determined by the boundary layers on both sides of the membrane in addition to the resistance of the membrane itself. Because of the diffusion coefficient differences between gases and liquids, the boundary layer on the gas side could be much thicker and more significant, but more prone to be minimised by adjusting the hydrodynamic conditions.

Upon the water vapor transferring to the gas side, the gas will quickly increase in humidity and become saturated, because the transfer rate of the vapor across the membrane is much faster (approximately 1000 times) than that of the gas [31]. As a consequence, vapor forms into droplets as observed in Fig. 7. Namely, the vapor pressure of the gas stream near the membrane is supposed to be the saturated vapor pressure at that temperature. In summary, mass transfer in SGMD has four consecutive processes: (a) vapor transfers through the active layer, (b) droplets form in the module, (c) droplets re-evaporate under gas stripping, and (d)

water vapor and/or droplets are swept out by the stripping gas. To the best of our knowledge, this is the first study reporting these important mass transfer phenomena on vapor condensation and re-evaporation in SGMD.

The phase change in terms of vapor condensation and droplet re-evaporation has significant influences on both heat and mass transfer. For example, at higher evaporation temperatures but lower gas flow rates, severe vapor condensation occurring on the gas side could cause module flooding and then SGMD could change into DCMD in which the mass transfer mechanism is considerably different. More details on the effect of vapor condensation on heat and mass transfer will be systematically investigated in our upcoming study entitled *Condensation, re-evaporation and associated heat transfer in membrane evaporation and sweeping gas membrane distillation*. Additionally, the finding of vapor saturation near the membrane interface on the gas side provides a new way for the evaluation of the vapor pressure on the gas side of the membrane. The findings of these phenomena in mass transfer offer significant insights not only for SGMD but also for other thermally driven membrane processes using stripping gases.

5. Conclusions

In this study, we systematically investigated the effects of evaporation temperature and hydrodynamic conditions on mass transfer in SGMD. The following interesting and important conclusions can be drawn from this work:

(1) Mass transfer in SGMD is principally determined by the evaporation temperature and the sweeping gas flow rate. The evaporation temperature provides almost exponentially increased vapor flux due to the exponential correlation between temperature and liquid partial vapor pressure. Higher sweeping gas flow rates result in higher gas vapor-holding capacity but

lower vapor partial pressure of the gas within the module, fundamentally leading to higher vapor flux.

(2) Mass transfer in SGMD is significantly influenced by the hydrodynamic conditions on both sides of the membrane through multiple effects, e.g. the boundary layer effect on both sides of the membrane and the temperature polarization effect.

(3) Because of the low vapor-holding capacity of a gas at low flow rates and the trans-membrane temperature drop, the sweeping gas becomes saturated in SGMD. Under saturation condition, water vapor forms droplets on the gas side and then the droplets are re-evaporated and swept out by the stripping gas.

Our novel findings on vapor condensation and droplet re-evaporation have great significance for both heat and mass transfer in SGMD, which will be presented in our next study.

Acknowledgements

We are grateful for financial support from the CSIRO's Energy Flagship. The authors also would like to thank Dr Erik Meuleman, Professor Mohamed Khayet and Professor Andrew Zydney for their valuable comments in preparing the manuscript. Special thanks also go to Dr Leigh Wardhaugh for his helpful suggestions about the experimental setup.

References

[1] K.W. Lawson, D.R. Lloyd, Membrane distillation, Journal of Membrane Science, 124 (1997) 1-25.

[2] M.S. El-Bourawi, Z. Ding, R. Ma, M. Khayet, A framework for better understanding membrane distillation separation process, Journal of Membrane Science, 285 (2006) 4-29.

[3] E. Curcio, G. Di Profio, E. Drioli, Membrane Distillation and Osmotic Distillation, in: D. Editor-in-Chief: Enrico, G. Lidietta (Eds.) Comprehensive Membrane Science and Engineering, Elsevier, Oxford, 2010, pp. 1-20.

[4] A. Alkhudhiri, N. Darwish, N. Hilal, Membrane distillation: A comprehensive review, Desalination, 287 (2012) 2-18.

[5] M. Khayet, Membranes and theoretical modeling of membrane distillation: A review, Advances in Colloid and Interface Science, 164 (2011) 56-88.

[6] A. Mourgues, N. Hengl, M.P. Belleville, D. Paolucci-Jeanjean, J. Sanchez, Membrane contactor with hydrophobic metallic membranes: 1. Modeling of coupled mass and heat transfers in membrane evaporation, Journal of Membrane Science, 355 (2010) 112-125.

[7] H. Mahmud, A. Kumar, R.M. Narbaitz, T. Matsuura, Mass transport in the membrane air-stripping process using microporous polypropylene hollow fibers: effect of toluene in aqueous feed, Journal of Membrane Science, 209 (2002) 207-219.

[8] H. Mahmud, A. Kumar, R.M. Narbaitz, T. Matsuura, A study of mass transfer in the membrane air-stripping process using microporous polyproplylene hollow fibers, Journal of Membrane Science, 179 (2000) 29-41.

[9] R.W. Schofield, A.G. Fane, C.J.D. Fell, Heat and mass transfer in membrane distillation, Journal of Membrane Science, 33 (1987) 299-313.

[10] R.W. Schofield, A.G. Fane, C.J.D. Fell, Gas and vapour transport through microporous membranes. II. Membrane distillation, Journal of Membrane Science, 53 (1990) 173-185.

[11] K.W. Lawson, D.R. Lloyd, Membrane distillation. II. Direct contact MD, Journal of Membrane Science, 120 (1996) 123-133.

[12] E. Curcio, E. Drioli, Membrane Distillation and Related Operations—A Review, Separation & Purification Reviews, 34 (2005) 35-86.

[13] J. Phattaranawik, R. Jiraratananon, A.G. Fane, Heat transport and membrane distillation coefficients in direct contact membrane distillation, Journal of Membrane Science, 212 (2003) 177-193.

[14] J. Zhang, S. Gray, J.-D. Li, Modelling heat and mass transfers in DCMD using compressible membranes, Journal of Membrane Science, 387–388 (2012) 7-16.

[15] J. Zhang, J.-D. Li, S. Gray, Effect of applied pressure on performance of PTFE membrane in DCMD, Journal of Membrane Science, 369 (2011) 514-525.

[16] M. Qtaishat, T. Matsuura, B. Kruczek, M. Khayet, Heat and mass transfer analysis in direct contact membrane distillation, Desalination, 219 (2008) 272-292.

[17] L. Basini, G. D'Angelo, M. Gobbi, G.C. Sarti, C. Gostoli, A desalination process through sweeping gas membrane distillation, Desalination, 64 (1987) 245-257.

[18] M. Khayet, P. Godino, J.I. Mengual, Nature of flow on sweeping gas membrane distillation, Journal of Membrane Science, 170 (2000) 243-255.

[19] M. Khayet, P. Godino, J.I. Mengual, Theory and experiments on sweeping gas membrane distillation, Journal of Membrane Science, 165 (2000) 261-272.

[20] M. Khayet, M.P. Godino, J.I. Mengual, Thermal boundary layers in sweeping gas membrane distillation processes, AIChE Journal, 48 (2002) 1488-1497.

[21] M. Khayet, M.P. Godino, J.I. Mengual, Theoretical and experimental studies on desalination using the sweeping gas membrane distillation method, Desalination, 157 (2003) 297-305.

[22] M. Khayet, C. Cojocaru, A. Baroudi, Modeling and optimization of sweeping gas membrane distillation, Desalination, 287 (2012) 159-166.

[23] M. Khayet, C. Cojocaru, Artificial neural network model for desalination by sweeping gas membrane distillation, Desalination, 308 (2013) 102-110.

[24] I.M. Smallwood, Solvent recovery handbook, Arnold, Paris, 1993.

[25] M. Gryta, M. Tomaszewska, Heat transport in the membrane distillation process, Journal of Membrane Science, 144 (1998) 211-222.

[26] H. Kuhn, H.D. Forstering, Principles of Physical Chemistry, Wiley, New York, 2000.

[27] E.L. Cussler, Diffusion: Mass Transfer in Fluid Systems (2nd ed.), Cambridge University Press, New York, 1997.

[28] J. Phattaranawik, R. Jiraratananon, A.G. Fane, Effect of pore size distribution and air flux on mass transport in direct contact membrane distillation, Journal of Membrane Science, 215 (2003) 75-85.

[29] W. Kast, C.R. Hohenthanner, Mass transfer within the gas-phase of porous media, International Journal of Heat and Mass Transfer, 43 (2000) 807-823.

[30] W.M. Haynes, CRC handbook of chemistry and physics, 94th Ed., 2013-2014.

[31] Y. Fang, P.J. Novak, R.M. Hozalski, E.L. Cussler, M.J. Semmens, Condensation studies in gas permeable membranes, Journal of Membrane Science, 231 (2004) 47-55.

Tables

Table 1

Knudsen numbers of typical MD membranes at different temperatures.

Temperature (°C)	K_n - 0.1 µm	K_n - 0.2 µm	K_n - 0.45 µm	K_n - 1.0 µm
20	0.99	0.49	0.22	0.10
25	1.01	0.50	0.22	0.10
30	1.02	0.51	0.23	0.10
35	1.04	0.52	0.23	0.10
40	1.06	0.53	0.23	0.11
45	1.07	0.54	0.24	0.11
50	1.09	0.54	0.24	0.11
55	1.11	0.55	0.25	0.11
60	1.12	0.56	0.25	0.11
65	1.14	0.57	0.25	0.11
70	1.16	0.58	0.26	0.12
75	1.17	0.59	0.26	0.12
80	1.19	0.60	0.26	0.12
85	1.21	0.60	0.27	0.12
90	1.22	0.61	0.27	0.12
95	1.24	0.62	0.28	0.12
100	1.26	0.63	0.28	0.13

Table 2

Properties of the PTFE membranes.

Membrane sample	[a] Nominal pore size (μm)	PTFE thickness (μm)	Support thickness (μm)	Total thickness (μm)	[a] Liquid entry pressure (kPa)	Water contact angle (°)	[a] Porosity (%)
A	0.1	20 ± 1	90 ± 1	110 ± 1	~ 170	109.9 ± 0.4	85~93
B	0.45	20 ± 1	140 ±1	160 ± 1	~ 120	120.3 ± 0.5	85~93

[a] Data provided by the manufacturer.

Table 3

Comparison of the saturated humidity ratio (HR_s) and the experimentally determined humidity ratio (HR_{ed}) based on Eq. (23) at the outlet of the sweeping gas at various temperatures.

Evaporation temperature (°C)	Membrane A - 0.1 µm				Membrane B - 0.45 µm			
	[a] $T_{g\text{-}out}$(°C)	[b] $P_{v\text{-}s}$ (kPa)	[b] HR_s (g/kg)	HR_{ed} (g/kg)	$T_{g\text{-}out}$(°C)	$P_{v\text{-}s}$ (kPa)	HR_s (g/kg)	HR_{ed} (g/kg)
35	27.9	3.77	24.9	43.0	29.4	4.11	27.2	68.8
45	36.0	5.96	40.2	74.6	37.3	6.40	43.4	100.4
55	44.8	9.52	66.7	123.4	46.1	10.18	71.8	173.6
65	53.3	14.55	107.9	176.4	56.4	16.88	128.6	258.2
75	63.0	22.93	188.1	261.0	65.3	25.42	215.4	385.8
80	68.2	28.9	256.6	344.2	69.9	31.11	285.0	481.9

[a] Measured outlet temperature of the sweeping gas;

[b] Simulated saturation vapor pressure/humidity at the corresponding temperature using the humidity calculation software from Vaisala, Finland.

Table 4

Comparison of the saturated humidity ratio (HR_s) and the experimentally determined humidity ratio (HR_{ed}) based on Eq. (23) at the outlet of the sweeping gas at various gas flow rates.

Gas flow rate (L/h)	Membrane A - 0.1 µm				Membrane B - 0.45 µm			
	[a] $T_{g\text{-}out}$(°C)	[b] $P_{v\text{-}s}$ (kPa)	[b] HR_s (g/kg)	HR_{ed} (g/kg)	$T_{g\text{-}out}$(°C)	$P_{v\text{-}s}$ (kPa)	HR_s (g/kg)	HR_{ed} (g/kg)
10	27.0	3.58	23.5	251.1	28.4	3.88	25.6	301.2
20	31.4	4.61	30.7	129.1	32.2	4.83	32.2	180.7
30	33.7	5.25	35.1	103.3	34.6	5.52	37.1	137.7
40	35.0	5.64	37.9	88.9	35.8	5.90	39.7	116.2
50	36.0	5.96	40.2	82.6	35.9	5.93	40.0	103.3
60	36.0	5.96	40.2	78.9	36.6	6.16	41.6	90.4
100	35.2	5.71	38.4	62.0	36.5	6.13	41.4	77.5
150	34.0	5.34	35.8	49.3	35.6	5.83	39.3	64.3
200	33.4	5.16	34.5	41.3	35.5	5.80	39.1	63.3
250	32.6	4.94	32.9	38.6	35.4	5.77	38.8	60.6

[a] Measured outlet temperature of the sweeping gas;

[b] Simulated saturation vapor pressure/humidity at the corresponding temperature using the humidity calculation software from Vaisala, Finland.

Table 5

Comparison of the saturated humidity ratio (HR_s) and the experimentally determined humidity ratio (HR_{ed}) based on Eq. (23) at the outlet of the sweeping gas at various liquid flow rates.

Liquid flow rate (L/h)	Membrane A - 0.1 µm				Membrane B - 0.45 µm			
	[a] $T_{g\text{-}out}$(°C)	[b] $P_{v\text{-}s}$ (kPa)	[b] HR_s (g/kg)	HR_{ed} (g/kg)	$T_{g\text{-}out}$(°C)	$P_{v\text{-}s}$ (kPa)	HR_s (g/kg)	HR_{ed} (g/kg)
10	35.7	5.87	39.5	63.1	36.7	6.20	41.9	88.9
20	36.1	6.00	40.5	73.1	37.2	6.37	43.1	91.8
30	36.5	6.13	41.4	81.8	37.3	6.40	43.4	97.5
40	36.6	6.16	41.6	88.9	37.5	6.47	43.9	103.3
50	37.0	6.30	42.6	94.7	37.4	6.44	43.6	107.6
60	36.7	6.20	41.9	97.5	37.7	6.54	44.4	110.4

[a] Measured outlet temperature of the sweeping gas;

[b] Simulated saturation vapor pressure/humidity at the corresponding temperature using the humidity calculation software from Vaisala, Finland.

Figure captions

Fig. 1. Schematic diagram of the bench-scale experimental setup for membrane evaporation. P = pressure gauge, T = thermal couple, H = humidity transmitter.

Fig. 2. Effect of evaporation temperature on vapor flux in SGMD. Constant conditions: dry nitrogen as the sweeping gas; inlet gas temperature 21 °C; gas flow rate 60 L/h; liquid flow rate 20 L/h; gas side pressure 0; liquid side pressure 13.8 kPa.

Fig. 3. Effect of gas flow rate on vapor flux in SGMD. Constant conditions: dry nitrogen as the sweeping gas; inlet gas temperature 21 °C; evaporation temperature 45 °C; liquid flow rate 20 L/h; gas side pressure 0; liquid side pressure 13.8 kPa.

Fig. 4. Effect of gas flow rate on the overall mass transfer cofficient in SGMD. Constant conditions: dry nitrogen as the sweeping gas; inlet gas temperature 21 °C; evaporation temperature 45 °C; liquid flow rate 20 L/h; gas side pressure 0; liquid side pressure 13.8 kPa. The overall mass transfer coefficient K is calculated according to Eq. (1), where the permeate vapor partial pressure (P_p) at the interface of the separation layer and sweeping gas is supposed to be equal to the saturation vapor pressure of the sweeping gas as the gas is saturated.

Fig. 5. Effect of liquid flow rate on vapor flux in membrane evaporation. Constant conditions: dry nitrogen as the sweeping gas; inlet gas temperature 21 °C; evaporation temperature 45 °C; gas flow rate 60 L/h; gas side pressure 0; liquid side pressure 13.8 kPa.

Fig. 6. Comparison of vapor flux using dry and humidified sweeping gases. Constant conditions: inlet gas temperature 21 °C; evaporation temperature 45 °C; liquid flow rate 20 L/h; gas side pressure 0; liquid side pressure 13.8 kPa.

Fig. 7. Photographs of the observed droplets on the support/backing layer of the membrane and in the membrane cell on the gas side.

Fig. 8. Schematic illustration of mass transfer across a porous membrane.

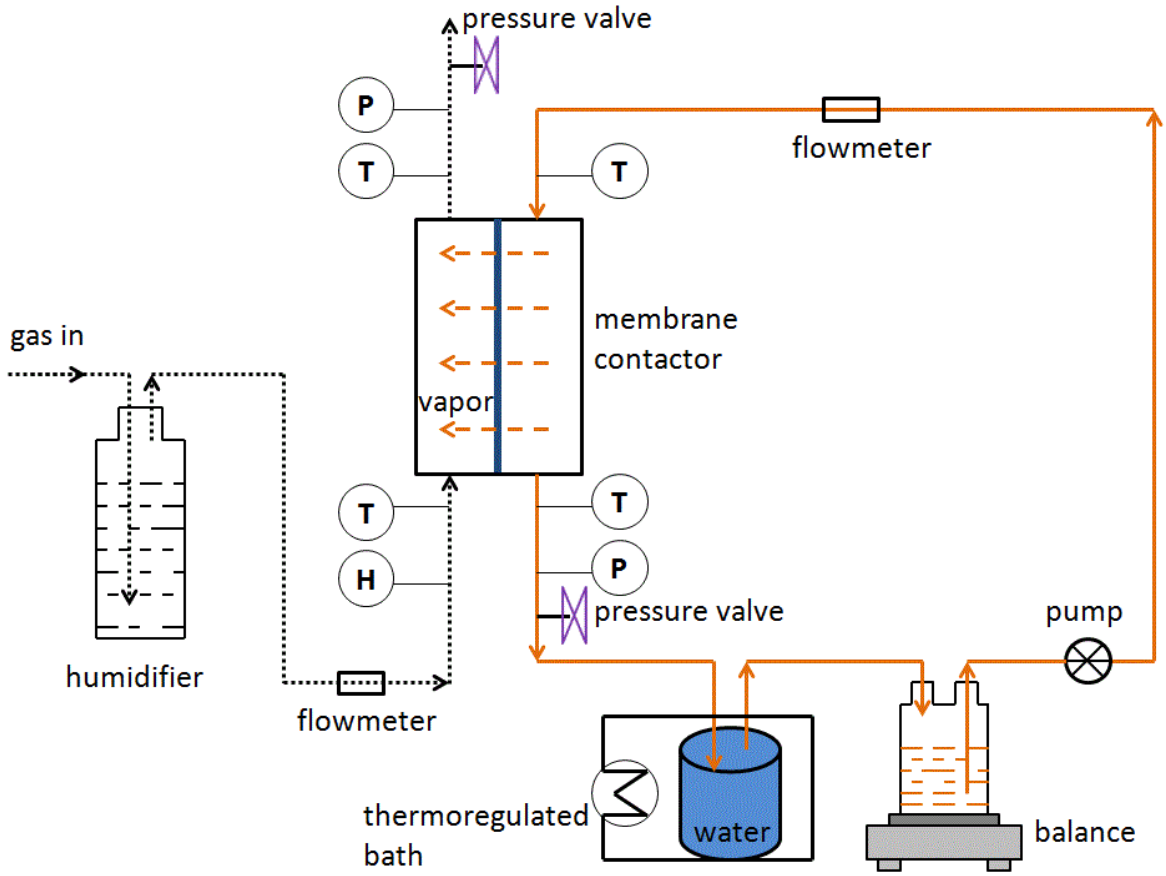

Fig. 1. Schematic diagram of the bench-scale experimental setup for membrane evaporation.

P = pressure gauge, T = thermal couple, H = humidity transmitter.

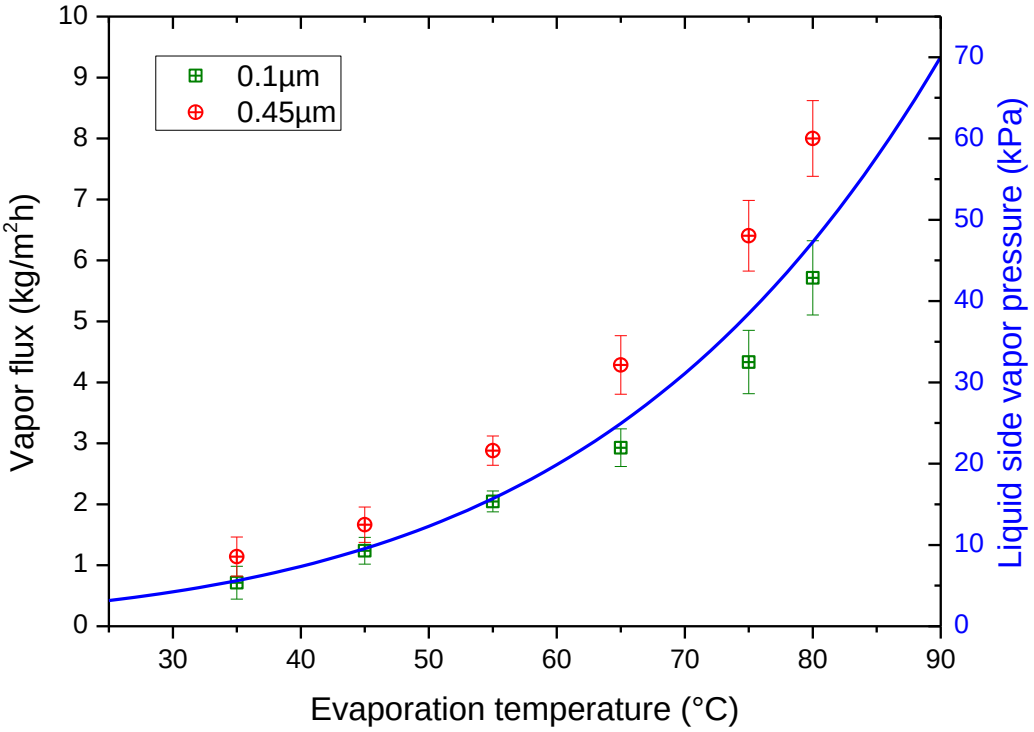

Fig. 2. Effect of evaporation temperature on vapor flux in SGMD. Constant conditions: dry nitrogen as the sweeping gas; inlet gas temperature 21 °C; gas flow rate 60 L/h; liquid flow rate 20 L/h; gas side pressure 0; liquid side pressure 13.8 kPa.

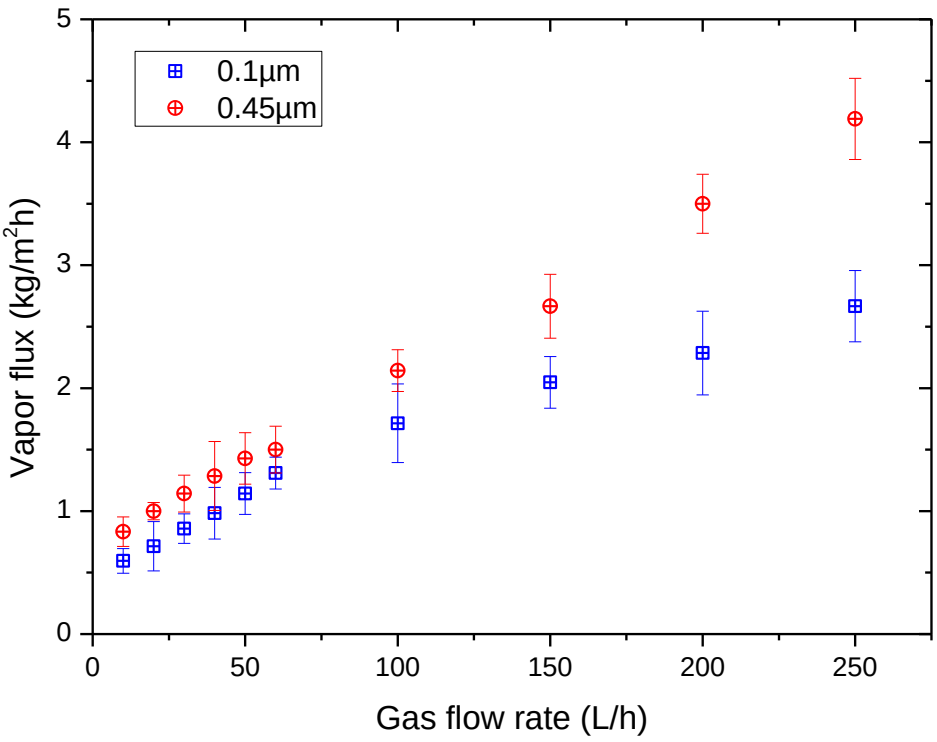

Fig. 3. Effect of gas flow rate on vapor flux in SGMD. Constant conditions: dry nitrogen as the sweeping gas; inlet gas temperature 21 °C; evaporation temperature 45 °C; liquid flow rate 20 L/h; gas side pressure 0; liquid side pressure 13.8 kPa.

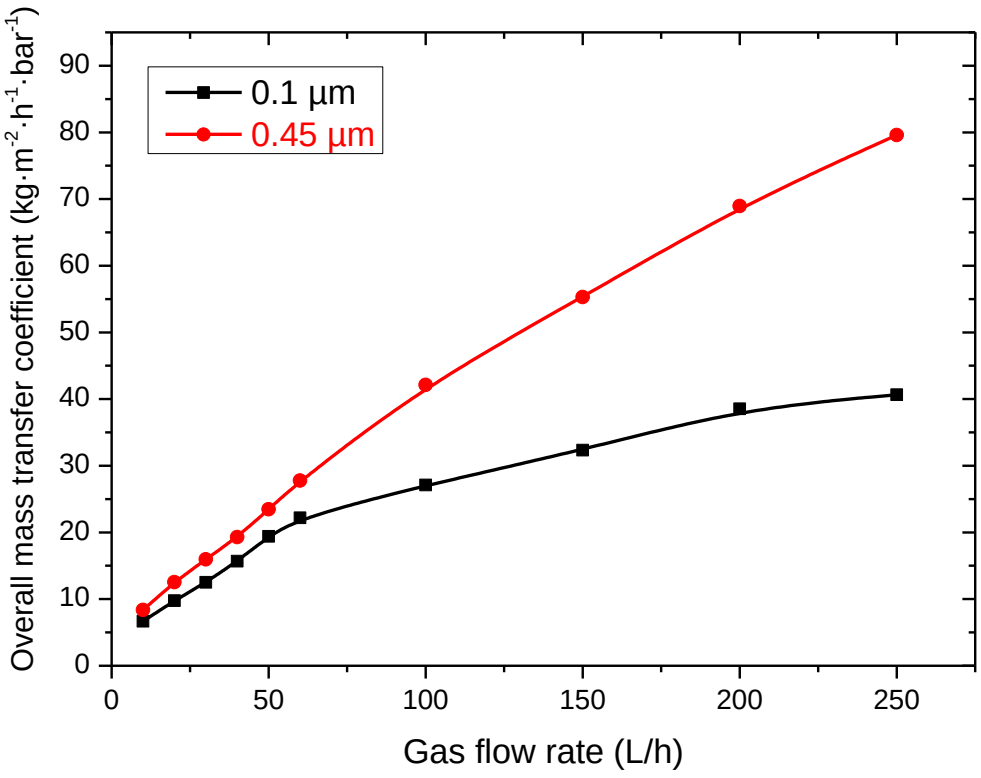

Fig. 4. Effect of gas flow rate on the overall mass transfer coefficient in SGMD. Constant conditions: dry nitrogen as the sweeping gas; inlet gas temperature 21 °C; evaporation temperature 45 °C; liquid flow rate 20 L/h; gas side pressure 0; liquid side pressure 13.8 kPa. The overall mass transfer coefficient K is calculated according to Eq. (1), where the permeate vapor partial pressure (P_p) at the interface of the separation layer and sweeping gas is supposed to be equal to the saturation vapor pressure of the sweeping gas as the gas is saturated.

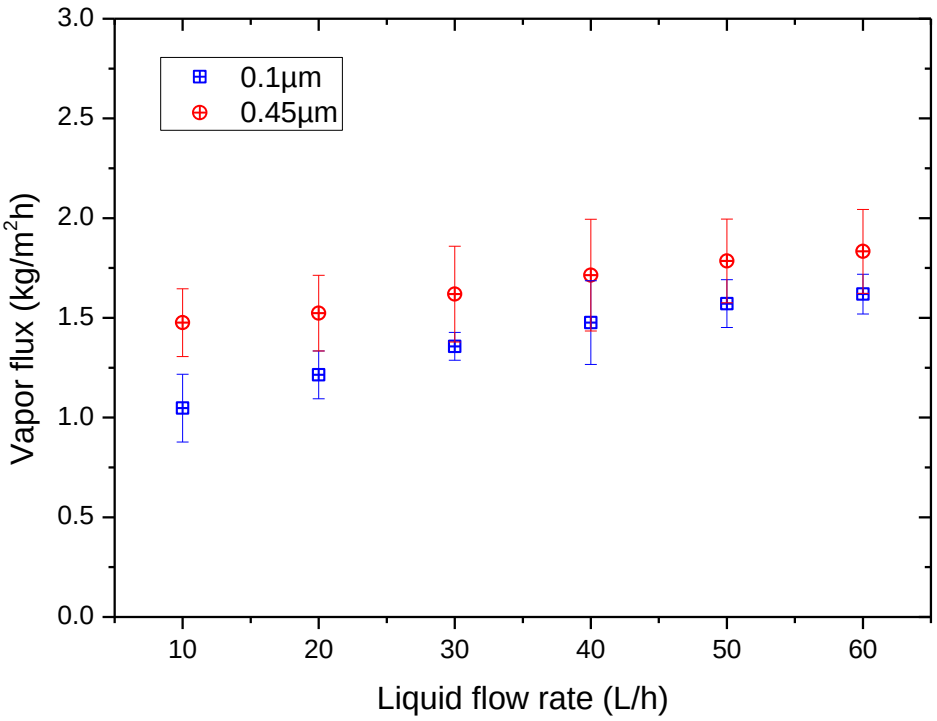

Fig. 5. Effect of liquid flow rate on vapor flux in membrane evaporation. Constant conditions: dry nitrogen as the sweeping gas; inlet gas temperature 21 °C; evaporation temperature 45 °C; gas flow rate 60 L/h; gas side pressure 0; liquid side pressure 13.8 kPa.

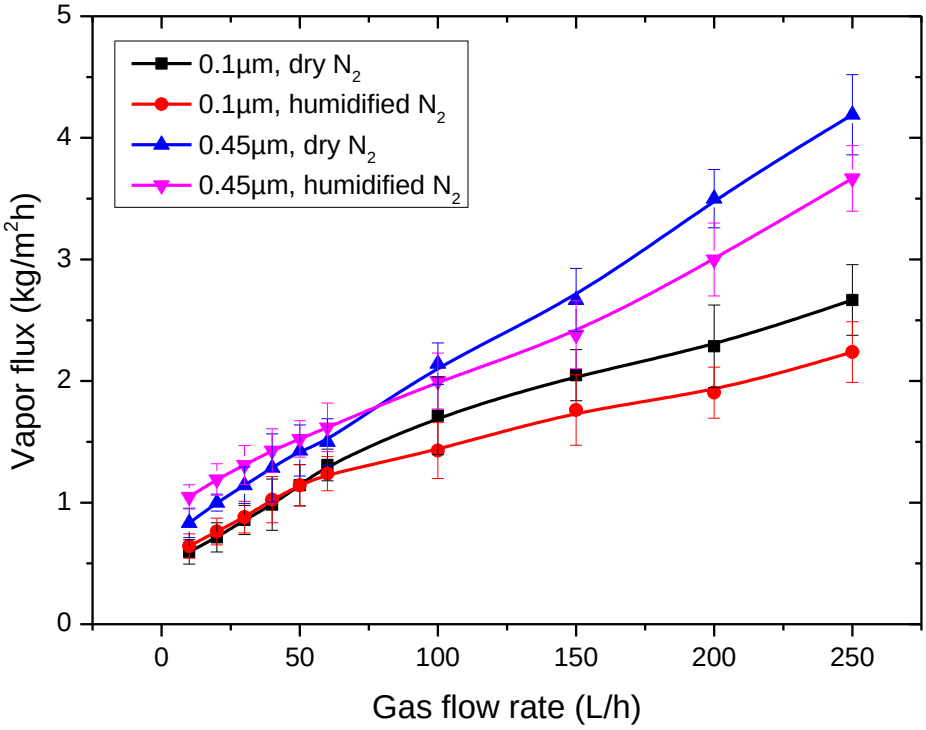

Fig. 6. Comparison of vapor flux using dry and humidified sweeping gases. Constant conditions: inlet gas temperature 21 °C; evaporation temperature 45 °C; liquid flow rate 20 L/h; gas side pressure 0; liquid side pressure 13.8 kPa.

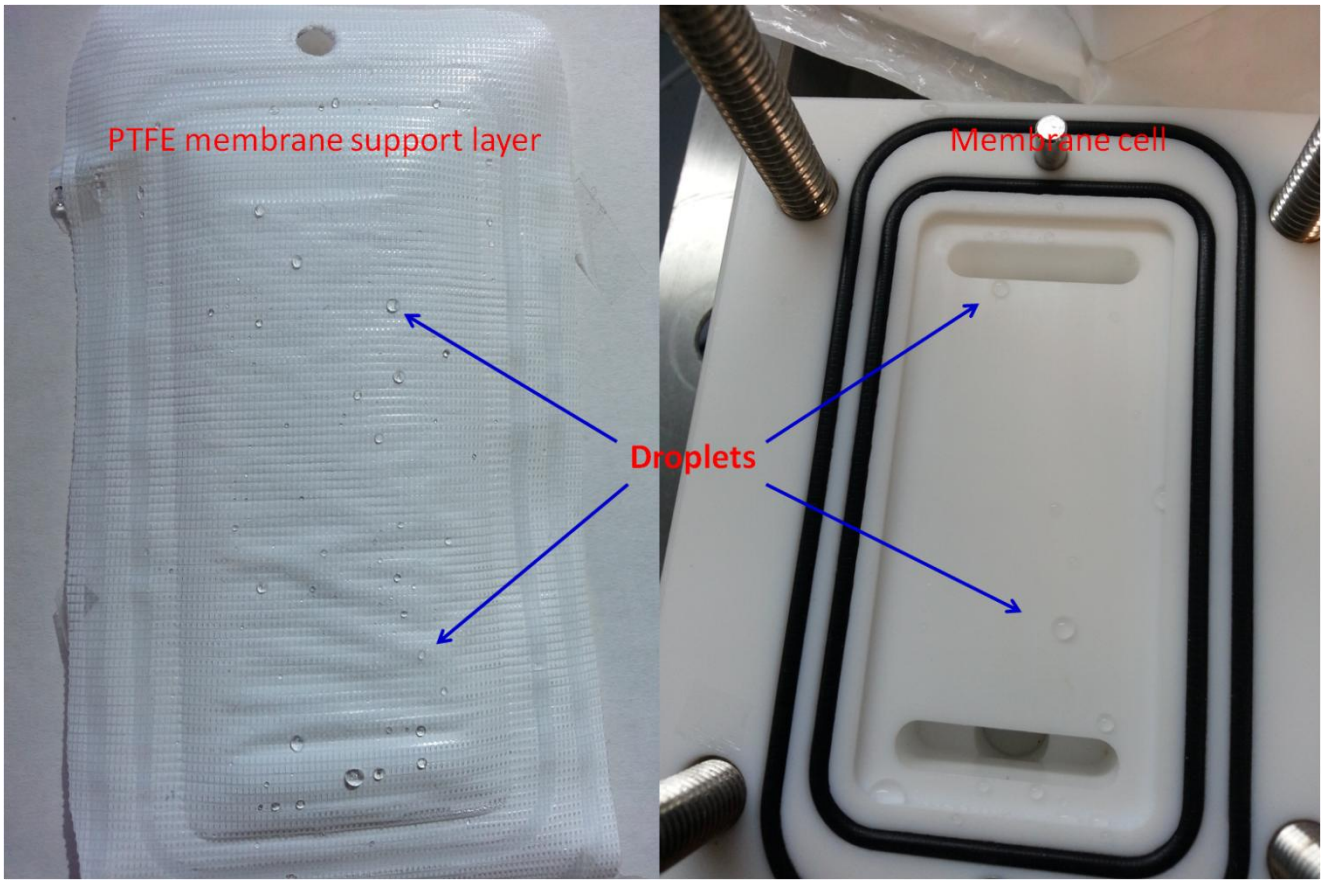

Fig. 7. Photographs of the observed droplets on the support/backing layer of the membrane and in the membrane cell on the gas side.

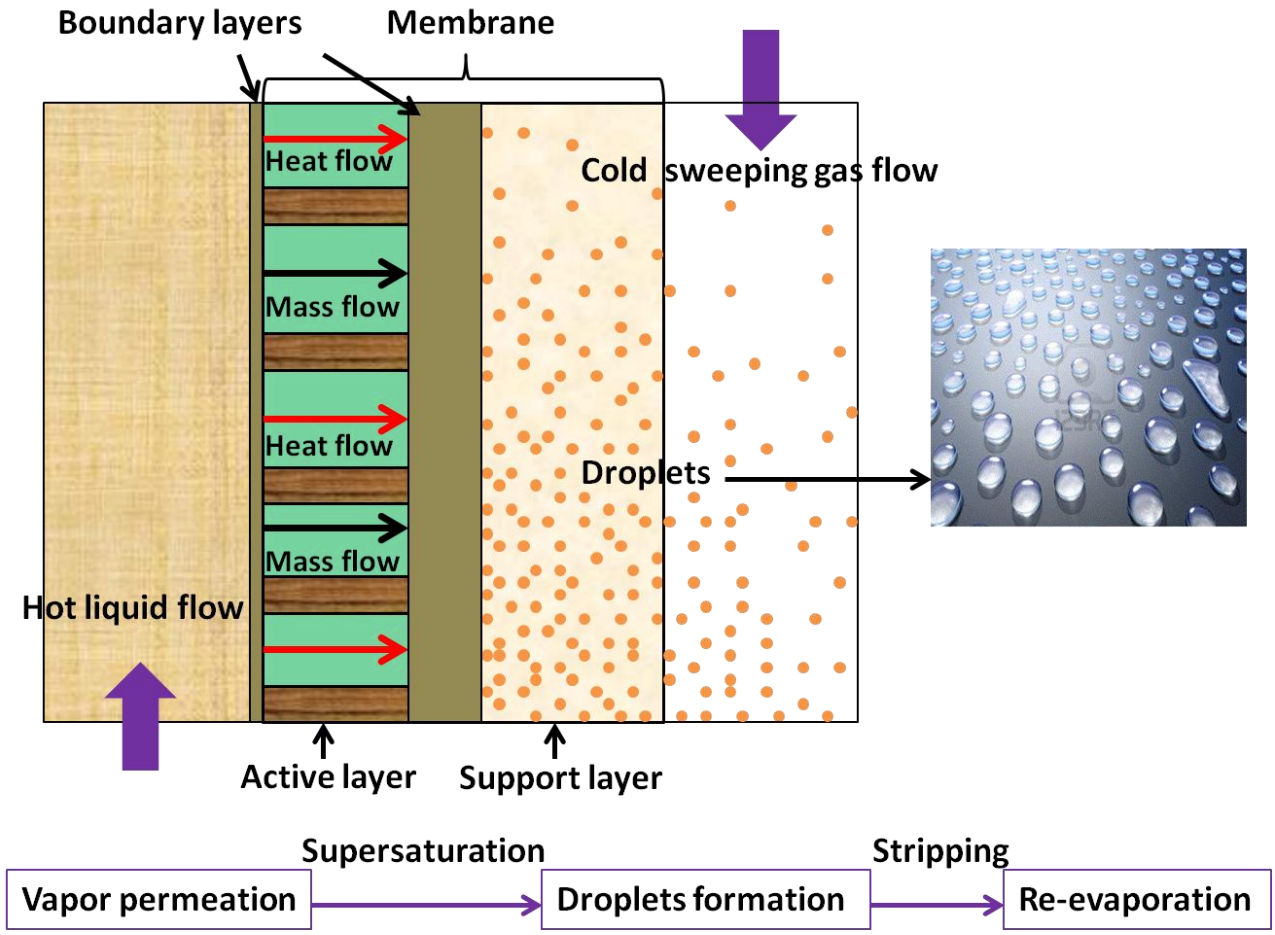

Fig. 8. Schematic illustration of mass transfer across a p